

Median Robust Extended Local Binary Pattern for Texture Classification

Li Liu, Songyang Lao, Paul W. Fieguth, *Member, IEEE*, Yulan Guo,
Xiaogang Wang, and Matti Pietikäinen, *Fellow, IEEE*

Abstract—Local binary patterns (LBP) are considered among the most computationally efficient high-performance texture features. However, the LBP method is very sensitive to image noise and is unable to capture macrostructure information. To best address these disadvantages, in this paper, we introduce a novel descriptor for texture classification, the median robust extended LBP (MRELBP). Different from the traditional LBP and many LBP variants, MRELBP compares regional image medians rather than raw image intensities. A multiscale LBP type descriptor is computed by efficiently comparing image medians over a novel sampling scheme, which can capture both microstructure and macrostructure texture information. A comprehensive evaluation on benchmark data sets reveals MRELBP’s high performance—robust to gray scale variations, rotation changes and noise—but at a low computational cost. MRELBP produces the best classification scores of 99.82%, 99.38%, and 99.77% on three popular Outex test suites. More importantly, MRELBP is shown to be highly robust to image noise, including Gaussian noise, Gaussian blur, salt-and-pepper noise, and random pixel corruption.

Index Terms—Texture descriptors, rotation invariance, local binary pattern (LBP), feature extraction, texture analysis.

I. INTRODUCTION

TEXTURE is an important characteristic of many types of images, ranging from large-scale multispectral remotely sensed data to microscopy. Texture classification, as one of the major problems in texture analysis, has been a long-standing research topic due to its significance both in understanding

Manuscript received August 12, 2015; revised November 12, 2015 and December 17, 2015; accepted January 22, 2016. Date of publication January 27, 2016; date of current version February 12, 2016. This work was supported in part by the National Natural Science Foundation of China under Grant 61201339 and Grant 61202336 and in part by the Open Project Program within the National Laboratory of Pattern Recognition. The associate editor coordinating the review of this manuscript and approving it for publication was Dr. Vladimir Stankovic.

L. Liu and S. Lao are with the Information System Engineering Key Laboratory, School of Information System and Management, National University of Defense Technology, Changsha 410073, China (e-mail: lilyliu_nudt@163.com; laosongyang@nudt.edu.cn).

P. W. Fieguth is with the Department of Systems Design Engineering, University of Waterloo, Waterloo, ON N2L 3G1, Canada (e-mail: pfieguth@uwaterloo.ca).

Y. Guo is with the School of Electronic Science and Engineering, National University of Defense Technology, Changsha 410073, China (e-mail: yulan.guo@nudt.edu.cn).

X. Wang is with the Department of Electronic Engineering, The Chinese University of Hong Kong, Hong Kong (e-mail: xgwang@ee.cuhk.edu.hk).

M. Pietikäinen is with the Center for Machine Vision Research, Department of Computer Science and Engineering, University of Oulu, Oulu 90014, Finland (e-mail: matti.pietikainen@ee.oulu.fi).

Color versions of one or more of the figures in this paper are available online at <http://ieeexplore.ieee.org>.

Digital Object Identifier 10.1109/TIP.2016.2522378

how the texture recognition process works in humans as well as in the important role it plays in the wide variety of applications of computer vision and image analysis [1], [2]. The many applications of texture classification include medical image analysis and understanding, object recognition, biometrics, content-based image retrieval, remote sensing, industrial inspection, and document classification.

As a classical pattern recognition problem, texture classification primarily consists of two critical subproblems: feature extraction and classifier designation [1], [2]. It is generally agreed that the extraction of powerful texture features plays a relatively more important role, since if poor features are used even the best classifier will fail to achieve good recognition results. Consequently, most research in texture classification focuses on the feature extraction part and numerous texture feature extraction methods have been developed, with excellent surveys given in [1]–[5]. Most existing methods have not, however, been capable of performing sufficiently well for real-world applications, which have demanding requirements including database size, nonideal environmental conditions, and running in real-time.

The inherent difficulty in extracting powerful texture features lies in balancing two competing goals: high-quality description and low computational complexity. High quality descriptors have to manage the tradeoff between distinctiveness, due to the wide range of texture classes, and robustness, due to large intraclass variations caused by variations in illumination, rotation, scale, blur, noise and occlusion. High speed descriptors and low dimensionality representation enable the entire application task to run in real-time. Many research efforts have been made to achieve either strict quality requirements or low computational speed.

Local Binary Patterns (LBP) [6] have emerged as one of the most prominent texture descriptors, attracting significant attention in the field of computer vision and image analysis due to their outstanding advantages:

- 1) ease of implementation,
- 2) invariance to monotonic illumination changes, and
- 3) low computational complexity.

Although originally proposed for texture analysis, the LBP method has been successfully applied to many diverse problems including dynamic texture recognition, remote sensing, fingerprint matching, visual inspection, image retrieval, biomedical image analysis, face image analysis, motion analysis, edge detection, and environment modeling [1], [7]–[11]. A large number of LBP variants [2] have been developed

to improve its robustness, discriminative power, and applicability.

With regards to discriminativeness, important examples include the Completed Local Binary Pattern (CLBP) [12], Extended Local Binary Pattern (ELBP) [10], Discriminative Completed Local Binary Pattern (*dis*CLBP) [34], Pairwise Rotation Invariant Cooccurrence Local Binary Pattern (PRICoLBP) [11] and the combination of Dominant Local Binary Pattern (DLBP) and Gabor filtering features [14]. However, despite the increase in discriminativeness, these LBP variants suffer in terms of robustness as they have minimal tolerance to image blur and noise corruption, and their feature dimensionality leads to increased computational complexity.

Similarly, the sensitivity of LBP to image degradation caused by blurring and noise has led to efforts including the Local Ternary Pattern (LTP) [15], Median Binary Pattern (MBP) [16], Local Phase Quantization (LPQ) [17], Fuzzy Local Binary Pattern (FLBP) [18], Noise Tolerant Local Binary Pattern (NTLBP) [19], Robust Local Binary Pattern (RLBP) [20] and Noise Resistant Local Binary Pattern (NRLBP) [21]. Although being more robust to image noise than traditional LBP, as has been remarked by others [1], [11], [21], [22] and observed in the experiments reports in this paper, the noise tolerance capability of these methods remains unsatisfactory.

Our recent ELBP approach [10] proposed four LBP-like descriptors — Center Intensity based LBP (ELBP_CI), Neighborhood Intensity based LBP (ELBP_NI), Radial Difference based LBP (ELBP_RD) and Angular Difference based LBP (ELBP_AD).¹ In that work the joint probability distribution of ELBP_CI, ELBP_NI and ELBP_RD (collectively referred as ELBP) produced good texture classification performance, however there remain some significant disadvantages:

- 1) Sensitivity to image blur and noise,
- 2) Failing to capture texture macrostructure, and
- 3) High feature dimensionality.

In order to overcome these shortcomings, in this paper we propose a conceptually simple, high-quality, and computationally efficient approach, the Median Robust Extended Local Binary Pattern (MRELBP), based on combining a median filter with multiresolution support. The key contributions of the proposed method are highlighted as follows:

- We introduce a novel sampling scheme which can encapsulate both microstructure and macrostructure information, inspired by DAISY [23], BRISK [24] and FREAK [25].
- We find that combining local medians with our novel sampling scheme proves to be very powerful texture feature.
- We evaluate the proposed method comprehensively on benchmark texture datasets from several different perspectives, including sampling parameters, encoding strategy, illumination invariance, rotation invariance, speed, discriminative power, and noise robustness.

¹In the original work [10], ELBP_CI, ELBP_NI, ELBP_RD and ELBP_AD are referred to as CI-LBP, NI-LBP, RD-LBP and AD-LBP respectively.

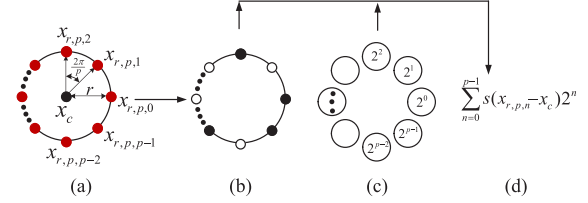


Fig. 1. (a) A typical (r, p) neighborhood used to derive an LBP-like operator: central pixel x_c and its p circularly and evenly spaced neighbors on a circle of radius r . (a) Original Pattern. (b) Binary Pattern. (c) Weights. (d) Decimal Value.

- The proposed method offers gray scale invariance, rotation invariance, no pretraining or parameter tuning, and offers exceptional discriminativeness and noise robustness when compared against eleven recent state-of-the-art LBP variants on ten benchmark texture datasets.

The remainder of this paper is organized as follows. Section II briefly discusses the related work. The derivation of the proposed approach operators and the classification framework are described in Section III. Experimental results are presented in Section IV. A preliminary version of this work appeared in [26].

II. RELATED WORK

A. Local Binary Pattern (LBP)

The LBP operator proposed by Ojala *et al.* [6] characterizes the spatial structure of a local image patch by encoding the differences between the pixel value of the central point and those of its neighbors, considering only the signs to form a binary pattern. The resulting decimal value of the generated binary pattern is then used to label the given pixel. Formally, as illustrated in Fig. 1, given a pixel x_c in the image, the LBP response is calculated by comparing its value with those of its p neighboring pixels $\{x_{r,p,n}\}_{n=0}^{p-1}$, evenly distributed in angle on a circle of radius r centered on x_c as

$$\text{LBP}_{r,p}(x_c) = \sum_{n=0}^{p-1} s(x_{r,p,n} - x_c) 2^n \quad (1)$$

where $s()$ is the sign function. If the coordinates of x_c are $(0, 0)$, then the coordinates of $x_{r,p,n}$ are given by $(-r \sin(2\pi n/p), r \cos(2\pi n/p))$. The gray values $x_{r,p,n}$ of neighbors which do not fall exactly in the center of pixels are estimated by interpolation.

A texture image can thus be characterized by the probability distribution of the 2^p LBP patterns. The LBP operator was extended to multiscale analysis to allow any radius and number of pixels in the neighborhood by varying parameters (r, p) .

To enhance the robustness to image rotation, a rotation invariant version $\text{LBP}_{r,p}^{ri}$ was proposed by grouping together all the binary patterns that are actually rotated versions of the same pattern [6]:

$$\text{LBP}_{r,p}^{ri} = \min\{\text{ROR}(\text{LBP}_{r,p}, i) | i = 0, 1, \dots, p-1\} \quad (2)$$

where $\text{ROR}(x, i)$ performs an i -step circular bit-wise right shift on x . Keeping only those rotationally-unique patterns leads to a significant reduction in feature dimensionality.

Ojala *et al.* [6] observed that certain LBP patterns represent the fundamental texture microstructures, and named these

ELBP

$$(b1) \text{ ELBP_CI}(x_c) = s(x_c - \beta)$$

$$\beta = \frac{1}{N} \sum_{c=0}^N x_c$$

$$(b2) \text{ ELBP_NI}_{r_2,8}(x_c) = \sum_{n=0}^7 s(x_{r_2,8,n} - \beta_{r_2,8}) 2^n$$

$$\beta_{r_2,8} = \frac{1}{8} \sum_{n=0}^7 x_{r_2,8,n}$$

$$(b3) \text{ ELBP_RD}_{r_2,r_1,8}(x_c) = \sum_{n=0}^7 s(x_{r_2,8,n} - x_{r_1,8,n}) 2^n$$

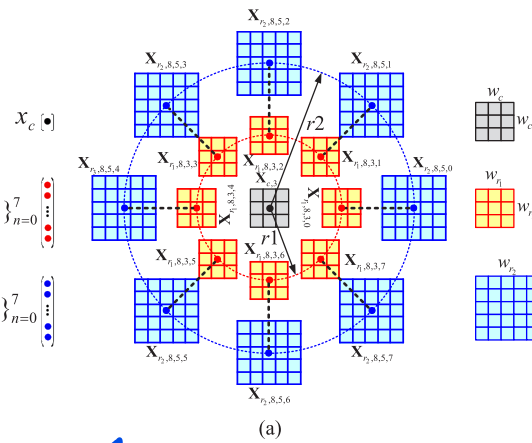


Fig. 2. Illustration for the proposed RELBP descriptor. The key difference between the ELBP [10] and the RELBP is that the only single pixel values are used in the ELBP, as opposed to a windowed or averaged approach in the RELBP.

patterns uniform patterns, those which have a U value of at most two:

$$U \leq 2$$

~~$U(LBP_{r,p}) = \sum_{n=0}^{p-1} |s(x_{r,p,n} - x_c) - s(x_{r,p,\text{mod}(n+1,p)} - x_c)|$~~ , such that $U(LBP_{r,p})$ counts the bitwise transitions from 0 to 1 or vice versa. The uniform descriptor, $LBP_{r,p}^{u2}$, has $p(p-1) + 3$ categories consisting of $p(p-1) + 2$ distinct uniform patterns and one nonuniform group containing all nonuniform patterns. Ojala *et al.* [6] proposed to further group the uniform patterns into $p + 1$ different rotation invariant categories, leading to the rotation invariant uniform descriptor $LBP_{r,p}^{riu2}$ with a much lower dimensionality of $p + 2$:

$$LBP_{r,p}^{riu2} = \begin{cases} \sum_{n=0}^{p-1} s(x_{r,p,n} - x_c), & \text{if } U(LBP_{r,p}) \leq 2 \\ p + 1, & \text{otherwise} \end{cases} \quad (3)$$

B. Extended Local Binary Pattern (ELBP)

Whereas LBP encodes only the relationship between a central point and its neighbors, ELBP is designed to encode distinctive spatial relationships in a local region and therefore contains more spatial information. ELBP [10] consist of three LBP-like descriptors ELBP_CI, ELBP_NI and ELBP_RD which explore information from the intensity of the center pixel, of its neighboring pixels, and radial differences, respectively.

The ELBP strategy is similar to the original LBP. The central pixel's intensity is thresholded

$$\text{ELBP_CI}(x_c) = s(x_c - \beta) \quad (4)$$

against β , the mean of the whole image.

Instead of using the gray value of the center pixel as the thresholding value, as used in LBP, ELBP_NI utilizes the average of the neighboring pixels' intensities to generate the binary pattern. As shown in the left panel of Fig. 2, ELBP_NI is defined as

$$\text{ELBP_NI}_{r,p}(x_c) = \sum_{n=0}^{p-1} s(x_{r,p,n} - \beta_{r,p}) 2^n \quad (5)$$

thresholded against the local mean $\beta_{r,p} = \frac{1}{p} \sum_{n=0}^{p-1} x_{r,p,n}$.

RELBP

$$(c1) \text{ RELBP_CI}(x_c) = s(\phi(\mathbf{X}_{c,3}) - \mu_3)$$

$$\mu_3 = \frac{1}{N} \sum_{c=0}^N \phi(\mathbf{X}_{c,3})$$

$$(c2) \text{ RELBP_NI}_{r_2,8,5}(x_c) = \sum_{n=0}^7 s(\phi(\mathbf{X}_{r_2,8,5,n}) - \mu_{r_2,8,5}) 2^n$$

$$\mu_{r_2,8,5} = \frac{1}{8} \sum_{n=0}^7 \phi(\mathbf{X}_{r_2,8,5,n})$$

$$(c3) \text{ RELBP_RD}_{r_2,r_1,8,5,3}(x_c) = \sum_{n=0}^7 s(\phi(\mathbf{X}_{r_2,8,5,n}) - \phi(\mathbf{X}_{r_1,8,3,n})) 2^n$$

In parallel to the intensity-based descriptors ELBP_NI and ELBP_CI, the ELBP_RD is derived from pixel *differences* in radial directions:

$$\text{ELBP_RD}_{r,r-1,p}(x_c) = \sum_{n=0}^{p-1} s(x_{r,p,n} - x_{r-1,p,n}) 2^n. \quad (6)$$

Similar to LBP, the grouping strategies for obtaining $LBP_{r,p}^{ri}$, $LBP_{r,p}^{u2}$ and $LBP_{r,p}^{riu2}$ can apply to ELBP_NI and ELBP_RD. Liu *et al.* [10] found that the $LBP_{r,p}^{riu2}$ led to good texture classification performance.

C. LBP Variants

Many extensions and modifications of LBP have been developed with an aim to increase its robustness and discriminativeness, with surveys given in [1], [27], and [28].

Changed Neighborhood Topology and Sampling: Orjuela-Vargas *et al.* [29] proposed Geometrical Local Textural Patterns (GLTP) which explores intensity changes on oriented neighborhoods. Nanni *et al.* [30] investigated the use of different neighborhood topologies (circle, ellipse, parabola, hyperbola and Archimedean spiral) and encodings in their research on LBP variants for medical image texture analysis. Hussain and Triggs [31] proposed Local Quantized Patterns (LQP) where a selection of possible geometries² are evaluated. These LBP variants aim to explore anisotropic information, not designed for rotation invariance. Wolf *et al.* [32] proposed Three Patch LBP (TPLBP) and Four Patch LBP (FPLBP) using averaged patch difference magnitudes.

Increasing Discriminative Power: There are three primary strategies to improve discriminative power: reclassifying the original LBP patterns to form more discriminative clusters, exploring cooccurrences, and combining with other texture descriptors. Yang and Wang [33] proposed Hamming LBP, which regroups nonuniform patterns based on

²Including horizontal, vertical, diagonal and antidiagonal strips of pixels, combinations of these like horizontal-vertical, diagonal-antidiagonal and horizontal-vertical-diagonal-antidiagonal, and traditional circular and disk-shaped regions.

Hamming distance instead of collecting them into a single bin. Guo *et al.* [34] proposed to learn discriminative rotation invariant patterns. Qi *et al.* [11] introduced Pairwise Rotation Invariant Cooccurrence LBP (PRICoLBP) which makes use of the cooccurrences of pairs of LBPs at certain relative displacements. Later on, Qi *et al.* proposed MultiScale Joint LBP (MSJLBP) [35] which also considers cooccurrences of LBPs, but from different scales. Ojala *et al.* [6] proposed a local contrast descriptor VAR to combine with LBP. Liao *et al.* [14] suggested the combination of Gabor filters and LBP. Ahonen *et al.* proposed an effective LBP Fourier histogram (LBPHF) to achieve global rotation invariance. Guo *et al.* [12] presented Completed LBP (CLBP) where the local differences are decomposed into signs and magnitudes. Wang *et al.* [36] proposed to combine LBP and a new descriptor called Local Neighboring Intensity Relationship Pattern (LNIRP) based on a sampling structure which combines pixel and patch to mimic the retinal sampling grid. LNIRP is similar to the descriptor AD-LBP presented in [10], but is based on second-order derivatives in the circular direction.

Enhancing Noise Robustness: Ahonen and Pietikänen introduced Soft LBP (SLBP) histograms [37], which enhances robustness by incorporating fuzzy membership in the representation of local texture primitives, and Iakovidis *et al.* [18] introduced Fuzzy LBP (FLBP), which allows multiple local binary patterns to be generated at each pixel position, both methods with a significant computational complexity. Ren *et al.* [21] proposed a much more efficient variant, the Noise Resistant LBP (NRLBP).

Tan and Triggs [15] introduced Local Ternary Patterns (LTP), which is more resistant to noise than LBP, but no longer strictly invariant to gray scale changes, and the selection of additional threshold values is not so simple. Liao *et al.* [14] introduced Dominant LBP (DLBP) to learn the most frequently occurred patterns to capture descriptive textural information, but which requires pretraining. Hafiane *et al.* [16] proposed Median Binary Pattern (MBP), where local binary patterns are determined by a localized thresholding against the local median. Ojansivu *et al.* [17] proposed Local Phase Quantization (LPQ), claiming robustness to image blur. Fathi and Naghsh-Nilchi [19] proposed Noise Tolerant LBP (NTLBP) where a circular majority voting filter and a new encoding strategy that regroups the nonuniform LBP patterns are presented, and Chen *et al.* [20] proposed Robust LBP (RLBP) [20] by changing the coding bit of LBP.

III. ROBUST EXTENDED LOCAL BINARY PATTERN

A. The Proposed RELBP

One drawback of the ELBP [10] is that it is very vulnerable to image noise, therefore the first strategy is to replace individual pixel intensities at a point with some representation over a region.

Notable methods along these lines include BRIEF [38], BRISK [24] and FREAK [25], where in all cases a binary descriptor vector is obtained by comparing the intensities of a

number of pairs of pixels after applying a Gaussian smoothing to reduce the noise sensitivity. However these approaches are based on keypoint detection, followed by a characterization of each keypoint. The rotation and scale invariance property of BRISK and FREAK depends on the detection of local regions of interest and the estimation of the dominant orientations. Thus the methods are used in a sparse approach, like that of Lazebnik *et al.* [39] and Zhang *et al.* [40], where salient regions are described with multiple descriptors such as SIFT, RIFT and SPIN. However, such sparse approaches have been demonstrated to be very complex and have been shown to be outperformed by dense approaches [41]–[43], upon which we are building in this paper.

We wish to consider the effect of replacing individual pixel gray values at sampled points with simple filter responses derived from source image patches centered on the sampling locations. The ELBP descriptor is now modified so that individual pixel intensities are replaced by a filter response $\phi()$, as illustrated in Fig. 2. However for comparison purposes the surrounding experimental context is held consistent between RELBP and ELBP: Images are normalized to zero mean and unit variance; the standard (riu^2) encoding scheme can be used; and the joint histogramming of RELBP_CI, $RELBP_{NI}^{riu^2}$ and $RELBP_{NI}^{riu^2}$ is used to represent a texture image. This new descriptor is referred to as $RELBP_{r,p}^{riu^2}$.

Formally, given a center pixel x_c and a patch filter ϕ , the RELBP_CI, RELBP_NI and RELBP_RD descriptors are defined as follows:

- 1) Center pixel representation:

$$RELBP_{CI}(x_c) = s(\phi(\mathbf{X}_{c,w}) - \mu_w) \quad (7)$$

the result of applying filter $\phi()$ to $\mathbf{X}_{c,w}$, the local patch of size $w \times w$ centered at the center pixel x_c , and μ_w denoting the mean of $\phi(\mathbf{X}_{c,w})$ over the whole image.

- 2) Neighbor representation:

$$RELBP_{NI,r,p}(x_c) = \sum_{n=0}^{p-1} s(\phi(\mathbf{X}_{r,p,w_r,n}) - \mu_{r,p,w_r}) 2^n$$

$$\mu_{r,p,w_r} = \frac{1}{p} \sum_{n=0}^{p-1} \phi(\mathbf{X}_{r,p,w_r,n}) \quad (8)$$

where $\mathbf{X}_{r,p,w_r,n}$ denotes a patch of size $w_r \times w_r$ centered on $x_{r,p,n}$.

- 3) Radial difference representation:

$$RELBP_{RD,r-1,p,w_r,w_{r-1}}(x_c) = \sum_{n=0}^{p-1} s(\phi(\mathbf{X}_{r,p,w_r,n}) - \phi(\mathbf{X}_{r-1,p,w_{r-1},n})) 2^n \quad (9)$$

where $\mathbf{X}_{r,p,w_r,n}$ and $\mathbf{X}_{r-1,p,w_{r-1},n}$ denote the patches centered at the neighboring pixels $x_{r,p,n}$ and $x_{r-1,p,n}$ respectively. $\{x_{r,p,n}\}_{n=0}^p$ represents the circularly and evenly spaced neighbors of the center pixel x_c at radius r .

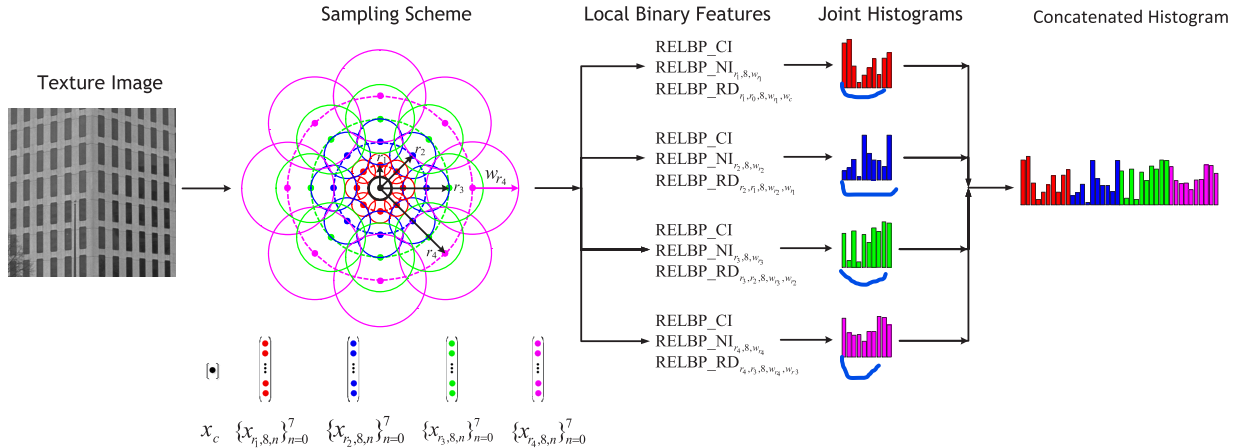


Fig. 3. Overview of the proposed multiscale RELBP descriptor. An example for illustrating RELBP sampling pattern is given with their corresponding support areas. Each solid circle represents a support area over which a corresponding filter response is computed to replace the gray value of a single sampled point. While this pattern resembles DAISY [23], BRISK [24] and FREAK [25], it is important to note that its use in the proposed MRELBP is different, as DAISY [23] was built specifically for dense matching, and BRISK [24] and FREAK [25] were designed for image matching.

In our proposed RELBP,³ we considered three basic choices for $\phi()$:

- Gaussian RELBP (GRELBP): sampling after Gaussian smoothing,
- Averaging RELBP (ARELBP): regional mean, and
- Median RELBP (MRELBP): regional median.

Clearly both the Gaussian and Averaged perform spatial averaging, and therefore noise reduction, however these methods are both linear, and therefore of only limited robustness, and will exhibit sensitivity to noise, particularly salt-and-pepper or corrupted-pixel noise. Our preference is therefore with the robust, nonlinear choice to apply a median filter as $\phi()$, to maximize the robustness of the representation to noise.

B. Encoding Scheme

In many LBP applications the rotation invariant uniform $riu2$ encoding scheme, defined in (3), has become standard. $LBP_{r,p}^{riu2}$ classifies all of the uniform LBPs into $p + 1$ rotation invariant groups and places all remaining nonuniform patterns into one single group. The rationale behind $LBP_{r,p}^{riu2}$ is that the uniform patterns occur much more frequently than nonuniform patterns in natural images [6], [7]. Bianconi and Fernández [44] presented a theoretical study on the relative occurrence of LBP patterns and argued that the high probability of occurrence of uniform patterns is likely to be a consequence of the mathematical structure of the LBP method rather than an intrinsic property of real textures.

However, the widespread use of $LBP_{r,p}^{riu2}$ has been challenged [13], [14], [19], [21], [45], with the claim that the uniform LBPs do not necessarily represent the most significant pattern features for certain classes of textured images, and that grouping all nonuniform patterns into one group may unnecessarily result in a loss of information. As a result, different encoding methods have been

proposed [13], [14], [19], [21], [45] that attempt to explore additional information present in the nonuniform LBP patterns. To test the information relevance of the encoding schemes for texture classification, we will compare several different encoding schemes, including a new one proposed in this paper:

- 1) $RELBP_{r,p}^{riu2}$: The traditional rotation invariant uniform encoding scheme defined in (3).
- 2) $RELBP_{r,p}^i$: The traditional rotation invariant encoding method defined in (2).
- 3) $RELBP_{r,p}^{ham}$: The encoding approach proposed by Zhou *et al.* [45], in which some nonuniform patterns are reclassified by minimizing a Hamming distance.
- 4) $RELBP_{r,p}^{faih}$: The encoding scheme proposed by Fathi and Naghsh-Nilchi [19], where all nonuniform patterns with four bitwise transitions (*i.e.* $U = 4$ in (3)) are classified based on the number of ones in the pattern, and the nonuniform patterns with $U > 4$ are grouped by U value.
- 5) $RELBP_{r,p}^{count}$: The method of [13], where all the LBP patterns are grouped into $p + 1$ different groups based on counting the number of ones.

Based on our observations we propose a new scheme $RELBP_{r,p}^{num}$, first dividing all LBPs into uniform and nonuniform according to the uniformity measure. Then as in $LBP_{r,p}^{riu2}$ the uniform patterns are divided into $p + 1$ rotation invariant groups. Finally, as opposed to $LBP_{r,p}^{riu2}$, we group the nonuniform pattern into $p - 3$ different groups based on the number of ones in the pattern. An example illustrating our approach is presented in Fig. 4.

C. MultiScale Analysis and Classification

Like most other LBP variants, by altering r and p we can realize operators for any quantization of the angular space and for any spatial resolution. A multiresolution analysis can therefore readily be accomplished by concatenating binary histograms from multiple resolutions into a single histogram.

We are proposing a multiscale sampling scheme, as illustrated in Fig. 3. The assumption of independence between

³For simplicity, we use RELBP to refer to any of the three descriptors GRELBP, ARELBP and MRELBP when we can do so unambiguously.

TABLE I

SUMMARY OF TEXTURE DATASETS USED IN OUR EXPERIMENTS.
 $\Theta_1 = \{5^\circ, 10^\circ, 15^\circ, 30^\circ, 45^\circ, 60^\circ, 75^\circ, 90^\circ\}$, $\Theta_2 = \{0^\circ, 5^\circ, 10^\circ, 15^\circ, 30^\circ, 45^\circ, 60^\circ, 75^\circ, 90^\circ\}$

Experiment # 1: Illumination and Rotation Invariance Evaluation

Texture Dataset	Texture Classes	Sample Size (pixels)	Images per Class	Number of Training Images	Number of Test Images	Description of Training and Testing
Outex_TC10	24	128 × 128	180	480 (20 * 24)	3840 (160 * 24)	Training: illuminants (inca), Rotations (0°) Testing: illuminants (inca), Rotations (Θ_1)
Outex_TC12_000	24	128 × 128	200	480 (20 * 24)	4320 (180 * 24)	Training: illuminants (inca), Rotations (0°)
Outex_TC36_000	108	128 × 128	200	2160 (20 * 108)	19440 (160 * 108)	Training: illuminants (inca), Rotations (0°) Testing: illuminants (l84), Rotations (Θ_2)
Outex_TC12_001	24	128 × 128	200	480 (20 * 24)	4320 (180 * 24)	Training: illuminants (inca), Rotations (0°)
Outex_TC36_001	108	128 × 128	200	2160 (20 * 108)	19440 (160 * 108)	Testing: illuminants (horizon), Rotations (Θ_2)

Experiment # 2: Noise Robustness Evaluation

Outex_TC11n	24	128 × 128	20	480 (20 * 24)	480 (20 * 24)	Training: illuminants (inca), Rotations (0°)
Outex_TC23n	68	128 × 128	20	1360 (20 * 68)	1360 (20 * 68)	Testing: Training images injected with Gaussian Noise
Outex_TC11b	24	128 × 128	20	480 (20 * 24)	480 (20 * 24)	Training: illuminants (inca), Rotations (0°)
Outex_TC23b	68	128 × 128	20	1360 (20 * 68)	1360 (20 * 68)	Testing: Training images blurred by Gaussian PSF
Outex_TC11s	24	128 × 128	20	480 (20 * 24)	480 (20 * 24)	Training: illuminants (inca), Rotations (0°)
Outex_TC23s	68	128 × 128	20	1360 (20 * 68)	1360 (20 * 68)	Testing: Training images injected with Salt-and-Pepper
Outex_TC11c	24	128 × 128	20	480 (20 * 24)	480 (20 * 24)	Training: illuminants (inca), Rotations (0°)
Outex_TC23c	68	128 × 128	20	1360 (20 * 68)	1360 (20 * 68)	Testing: Training images with Random Pixel Corruption

Experiment # 3: Robustness to Complex Variations Evaluation

Texture Dataset	Texture Classes	Sample Size (pixels)	Images per Class	Number of Training Images	Number of Test Images	Image Rotation Variation	Illumination Variation	Scale Variation	Significant Viewpoint
KTH-TIPS2b	11	200 × 200	432	3564 (324 * 11)	1188 (108 * 11)	✓	✓	✓	
UMD	25	1280 × 960	40	500 (20 * 25)	500 (20 * 25)	✓	✓	✓	✓
CUReT	61	200 × 200	92	2806 (46 * 61)	2806 (46 * 61)	✓	✓		
ALOT	250	384 × 256	100	12500 (50 * 250)	12500 (50 * 250)	✓	✓		

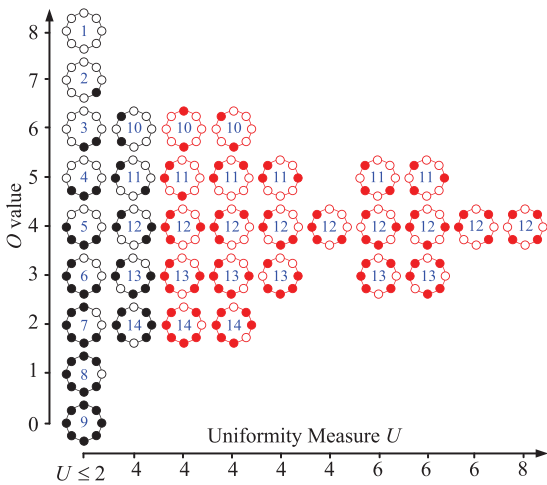


Fig. 4. $LBP_{r,8}^{num}$: Filled and empty circles correspond to bit values of 0 and 1 in $lbp_{r,8}$ operator. The numbers inside each pattern correspond to their unique category labels. The 14 categories in the number LBP scheme partitions the uniform patterns into 9 rotation-invariant groups and the nonuniform patterns into 5 different groups according to the O value (*i.e.* the number of 1s in the pattern).

texture features from different scales does not hold, however the estimation of large joint probabilities is also not feasible due to the computational complexity of large multidimensional histograms. Therefore we propose to generate the histogram feature as the concatenation over multiple scales.

While this pattern resembles the DAISY [23], BRISK [24] and FREAK [25], it is important to note that its use in MRELBP is entirely different, as they all applied Gaussian smoothing, DAISY [23] was built specifically for dense matching, and BRISK [24] and FREAK [25] were designed for image matching. Finally, the parameters controlling the shape of such sampling pattern are different for all three descriptors RELBP, BRISK and FREAK.

IV. EXPERIMENTAL EVALUATION

For the overall framework of the proposed approach, the actual classification is performed via the simple Nearest Neighbor Classifier (NNC), applied to the normalized MRELBP histogram feature vectors, using the χ^2 distance metric as in [12], [43], and [46]. Furthermore, results obtained with a more sophisticated classifier — support vector machines (SVM) [47], are also provided.

A. Image Data and Experimental Setup

We demonstrate the performance of our approach with three different problems of robust texture classification by conducting extensive experiments on a number of publicly available datasets, summarized in Table I, derived from the four most commonly used texture sources: Outex [48], CUReT [41], UMD [49], KTHTIPS2b [50] and ALOT [51].

Experiment #1: Experiment #1 tests robustness to gray scale and rotation variations. Outex [48] contains a large collection of surface textures captured under different conditions, which facilitates construction of a wide range of texture analysis problems. By selecting 24 different homogeneous texture classes from the Outex database, Ojala *et al.* [6] created three test suites Outex_TC10, Outex_TC12_000 and Outex_TC12_001 (summarized in Table I) which have been widely used as benchmark datasets for the evaluation of rotation and illumination invariant texture classification approaches. In addition, we selected 108 different texture classes, shown in Fig.5, to create two more challenging test suites Outex_TC36_000 and Outex_TC36_001.

Experiment #2: Experiment #2 tests robustness to random noise corruption, including Gaussian noise, image blurring, salt-and-pepper noise, and random pixel corruption, the same noise types tested in [52]. We use only the noise-free texture images for training and test on the noisy data, as summarized

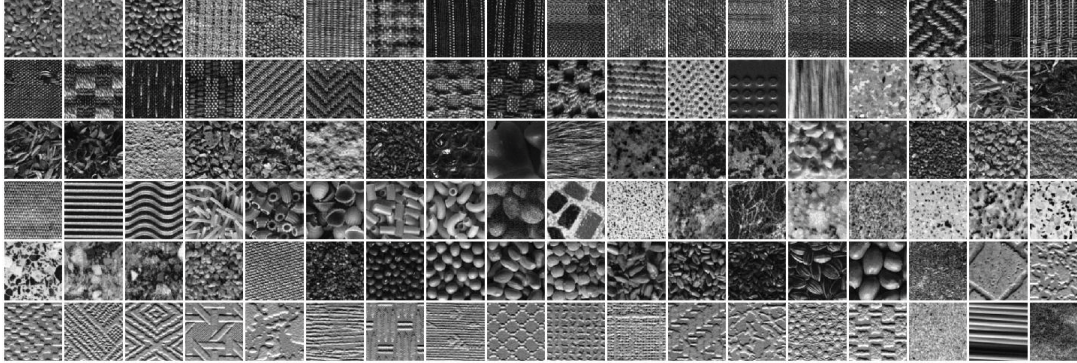


Fig. 5. The 108 texture classes from the Outex_TC36 datasets.

in Table I. The test suites are based on Outex_TC11n and Outex_TC23n, which have 24 and 68 texture classes, respectively. The noise parameters include Gaussian noise standard deviation σ , Gaussian blur standard deviation σ , Salt-and-Pepper noise density ρ , and pixel corruption density v .

Experiment # 3: Experiment #3 is carried out to measure robustness to more complex environment changes, including variations in viewpoint, scaling, illumination and rotation, based on the CURET, UMD, KTHTIPS2b and ALOT databases.

For the CURET database we use the same subset of images which has been previously used in [12], [13], [41], [43]: 61 texture classes each with 92 images under varying illumination direction but at a constant scale. It has been argued [41], [53], [54] that this scale constancy is a major drawback of CURET, leading to KTHTIPS2b [50], [54], with 3 viewing angles, 4 illuminants, and 9 different scales. The UMD database [49] consists of high resolution images, with arbitrary rotations, significant viewpoint changes and scale differences present. The ALOT dataset [51] consists of 250 classes each of which has 100 samples. We resize images in ALOT to obtain lower resolution (384×256). ALOT is challenging as it represents a significantly larger number of classes (250) compared to UMD (25) and has very strong illumination change (8 levels of illumination). The viewpoint change is however less dramatic compared to UMD. For CURET, UMD and ALOT, half of the class samples were selected at random for training and the remaining half for testing. For KTHTIPS2b, we follow the training and testing scheme of [54]: training on three samples and testing on the remainder.

B. Methods in Comparison and Implementation Details

We will be performing comprehensive experimental comparisons of our approach with eleven recent state-of-the-art LBP variants. Unless otherwise specified the $riu2$ encoding and (r, p) parameters $(1, 8) + (2, 16) + (3, 24)$ are used, which is the setting recommended by nearly all of the comparison methods.

- 1) ELBP [10]: The joint histogram of ELBP_CI, $ELBP_{NI}^{riu2}$ and $ELBP_{RD}^{riu2}$.

- 2) LBP [6]: The traditional rotation invariant uniform feature $LBP_{r,p}^{riu2}$ proposed by Ojala *et al.* [6].
- 3) CLBP [12]: The joint histogram of CLBP_C, $CLBP_{S}^{riu2}$ and $CLBP_{M}^{riu2}$.
- 4) LTP [15]: The recommended $LTP_{r,p}^{riu2}$ is used. LTP is claimed to be more robust to noise than LBP.
- 5) disCLBP [34]: Due to the high dimensionality of the descriptor at larger scales, we use a three-scale descriptor $dis(S+M)_{r,p}^{ri}$ as recommended by the authors.
- 6) MBP [16]: We implemented a multiscale $MBP_{r,p}^{riu2}$ descriptor $((1, 8) + (2, 16) + (3, 24))$, although Hafiane *et al.* [16] only examined the first scale $(r, p) = (1, 8)$ in their original paper.
- 7) NRLBP [21]: We implemented a multiresolution $NRLBP_{r,p}^{riu2}$ descriptor, although Ren *et al.* [21] only evaluated the first scale in their original paper. The number of neighboring points p is held fixed at 8 for each radius r , because the extraction of the NRLBP feature requires a large lookup table of size 3^p .
- 8) NTLBP $_{r,p,k}^{\text{faith}}$ [19]: Implemented in a multiscale form $NTLBP_{r,p,k}^{\text{faith}}$ ⁴ as suggested by the authors. Parameter k acts as the size of kernel in the filter, controlling the number of noisy bits that should be filtered, which is set to 1, 3 and 4 for $p = 8, 16$ and 24, respectively, as suggested in [19].
- 9) PRICoLBP [11]: The multiscale and multiorientation PRICoLBP $_g$ descriptor is used, with parameters as recommended by the authors.
- 10) MSJLBP [35]: The multiscale joint encoding of LBP proposed in [35], similar to PRICoLBP. Following the authors, (r, p) of $(1, 8), (2, 8), (3, 8)$ is used.
- 11) COV-LBPD [22]: The approach by combining LBP difference and feature correlation.

Each texture sample is preprocessed, normalized to zero mean and unit standard deviation. For the CURET, UMD and KTHTIPS2b databases, all results are reported over 100 random partitionings of training and testing sets. For SVM classification, we use the publicly available LibSVM library [47]. The parameters C and γ are searched exponentially in the ranges $[2^{-5}, 2^{18}]$ and $[2^{-15}, 2^8]$, respectively,

⁴ $NTLBP_{1,8,1}^{\text{faith}} + NTLBP_{2,16,3}^{\text{faith}} + NTLBP_{3,24,4}^{\text{faith}}$.

TABLE II
RESULTS (%) ON THREE BENCHMARK OUTEX TEST SUITES. THE PARAMETERS w_c AND w_r INVOLVED IN RELBP ARE SET AS $w_c = 3$ AND $w_r = (3, 3, 5, 7)$

(r, p)	(1,8)				(3,8)				(5,8)				(7,8)			
Method	TC10	TC12		Mean	TC10	TC12		Mean	TC10	TC12		Mean	TC10	TC12		Mean
		tl84	horizon			tl84	horizon			tl84	horizon			tl84	horizon	
MRELBP _{r,p} ^{riu2}	90.83	86.02	87.87	88.24	99.48	98.26	96.94	98.23	97.40	94.91	94.70	95.67	94.19	92.01	92.38	92.86
MRELBP_NI _{r,p} ^{riu2}	77.50	70.09	67.99	71.86	81.41	72.62	73.19	75.74	66.20	59.91	60.51	62.20	67.16	59.28	61.50	62.65
MRELBP_RD _{r,p} ^{riu2}	76.88	59.79	58.73	65.13	88.33	82.04	81.34	83.90	79.51	73.33	70.65	74.50	70.31	57.87	59.03	62.40
LBP _{r,p} ^{riu2} [6]	84.71	65.46	64.47	71.55	86.12	79.98	76.50	80.87	70.96	63.89	63.47	66.11	59.14	55.51	57.13	57.26
ELBP _{r,p} ^{riu2} [10]	96.41	91.30	92.87	93.52	99.09	97.78	95.69	97.52	93.91	90.28	89.54	91.24	81.48	75.49	76.62	77.86
ELBP_NI _{r,p} ^{riu2} [10]	76.51	59.12	56.20	63.94	80.18	70.56	67.01	72.58	72.37	63.13	64.65	66.72	67.71	58.56	61.97	62.75
ELBP_RD _{r,p} ^{riu2} [10]	84.71	65.46	64.47	71.55	81.48	74.91	74.63	77.01	69.69	69.00	60.21	66.30	51.85	51.20	50.58	51.21
(r, p)	(1,8)+(3,8)				(1,8)+(3,8)+(5,8)				(1,8)+(3,8)+(5,8)+(7,8)				(3,8)+(5,8)+(7,8)			
Method	TC10	TC12		Mean	TC10	TC12		Mean	TC10	TC12		Mean	TC10	TC12		Mean
		tl84	horizon			tl84	horizon			tl84	horizon			tl84	horizon	
MRELBP _{r,p} ^{riu2}	98.39	97.06	97.20	97.55	99.30	98.77	98.77	98.95	99.38	99.17	99.51	99.35	99.58	98.82	99.35	99.25
MRELBP_NI _{r,p} ^{riu2}	88.65	82.82	81.39	84.29	91.80	85.69	86.41	87.97	93.33	89.77	90.69	91.27	91.54	86.78	88.38	88.90
MRELBP_RD _{r,p} ^{riu2}	93.52	83.91	84.68	87.37	94.95	88.59	89.05	90.86	95.83	89.72	91.16	92.24	95.52	88.89	90.05	91.49
LBP _{r,p} ^{riu2} [10]	95.42	88.73	82.15	88.77	97.03	90.23	86.57	91.28	93.02	88.59	87.04	89.55	85.86	81.06	81.20	82.71
ELBP _{r,p} ^{riu2} [10]	99.32	97.92	97.59	98.28	99.51	98.54	97.64	98.56	99.45	97.99	97.78	98.41	97.76	96.34	95.81	96.64
ELBP_NI _{r,p} ^{riu2} [10]	91.25	81.20	75.46	82.64	94.24	85.21	84.65	88.04	94.27	89.24	87.85	90.45	87.79	83.26	82.85	84.63
ELBP_RD _{r,p} ^{riu2} [10]	93.54	86.85	84.84	88.41	92.01	87.78	84.14	87.98	85.65	83.68	81.34	83.56	79.30	75.88	74.28	76.49

with a step size of 2¹ to probe the highest classification rate; in our experiments setting $C = 10^6$ and $\gamma = 0.01$ give very good performance. For ELBP, LBP, CLBP, *dis*CLBP, PRICoLBP_g and COV-LBPD, we use the code provided by the original authors.

C. Experimental Tests

We wish to test the proposed method from seven different perspectives: gray scale invariance, rotation invariance, multiscale analysis, template setting, discriminative power, noise robustness, and encoding strategy.

1) *Regional vs. Pointwise*: Table II presents the results for the three test suites Outex_TC10, Outex_TC12_000 and Outex_TC12_001 in detail, comparing the proposed regional/multiscale MRELBP with pointwise ELBP. The results of LBP are included as a baseline.

Firstly, the proposed MRELBP_RD_{r,8}^{riu2} improves the performance over ELBP_RD_{r,8}^{riu2} considerably, with the lone exception at (1, 8), where the drop of performance may be due to too much overlapping of the sampling pattern near the center. The proposed MRELBP_NI_{r,8}^{riu2} also improved the performance in general, but not so significantly as MRELBP_RD_{r,8}^{riu2}. The joint descriptor MRELBP_{r,8}^{riu2} proved to be much more powerful and significantly outperformed ELBP_{r,8}^{riu2}.

Secondly, the use of multiscale offers significant improvements over single-scale analysis. The striking performance of multiscale MRELBP_{r,p}^{riu2} for the classification of texture with great illumination and rotation changes clearly demonstrates that the concatenated marginal joint distributions of MRELBP_CI, MRELBP_NI_{r,p}^{riu2} and MRELBP_RD_{r,p}^{riu2} turns out to be a very powerful representation of image texture and to be robust to gray scale and rotation variations. These results firmly demonstrate that the approach is making effective use of microstructure and the interactions between more

distant pixels. Therefore, in all further experiments we will only report multiscale results.

Table III presents the multiscale results for all three proposed descriptors GRELBP, ARELBP and MRELBP, in comparison with ELBP and LBP. For the parameter pair (r, p) , we tested the commonly employed (1,8), (3,16), (5,24), (7,24) [6], [12], [34] versus a fixed $p = 8$ at all scales. Although the higher dimensionality of the former scheme offered improved results for some of the individual descriptors, the joint descriptors all perform similarly under both settings, and all give very high classification scores on the three Outex test suites.

However because the feature dimensionality of the proposed RELBP_{r,p}^{riu2} at a single resolution is $2(p + 2)(p + 2)$, the former, higher-dimensional scheme results in a feature dimensionality of 3552, whereas a fixed $p = 8$ corresponds to a much lower dimensionality of only 800. Therefore, considering the similar classification performance given by the two schemes, we propose to fix the the number of sampling neighbors to $p = 8$ at each scale in our remaining experiments.

2) *GRELBP vs. ARELBP vs. MRELBP*: Table IV shows the noise robustness performance given the four noise types described in Section IV-A. It is very clear that the nonlinear, robust behaviour of the median filter leads MRELBP to be the clear winner in noise robustness, particularly in the cases of Salt-and-Pepper noise and random pixel corruption. The classification results are particularly impressive keeping in mind that the training images were all noise-free.

Based on the striking noise robustness results, the MRELBP strategy performs by far the best, and therefore it is our proposed choice for further evaluation.

3) *Template Setting*: The main parameters involved in the proposed MRELBP descriptor are the sampling radii r , the size of the center patch $w_c \times w_c$, and the size of the neighboring

TABLE III

CLASSIFICATION SCORES (%) ON Outex_TC10, Outex_TC12000 AND Outex_TC12001 TEST SUITES. THE PARAMETERS w_c AND w_r INVOLVED IN RELBP ARE SET AS $w_c = 3$ AND $w_r = (3, 3, 5, 7)$

(r, p)	(1,8)+(3,8)				(1,8)+(3,8)+(5,8)				(1,8)+(3,8)+(5,8)+(7,8)			
Method	TC10	TC12		Mean	TC10	TC12		Mean	TC10	TC12		Mean
		tl84	horizon			tl84	horizon			tl84	horizon	
GRELB $P^{riu2}_{r,p}$	99.71	98.68	98.77	99.06	99.79	99.28	99.40	99.49	99.82	99.03	99.65	99.50
GRELB $N^{riu2}_{r,p}$	87.40	77.87	79.03	81.43	87.21	83.03	81.92	84.06	87.40	83.54	84.07	85.00
GRELB $R^{riu2}_{r,p}$	93.65	87.08	87.69	89.47	96.07	90.21	90.44	92.24	95.81	90.56	91.99	92.78
MRELB $P^{riu2}_{r,p}$	98.39	97.06	97.20	97.55	99.30	98.77	98.77	98.95	99.38	99.17	99.51	99.35
MRELB $N^{riu2}_{r,p}$	88.65	82.82	81.39	84.29	91.80	85.69	86.41	87.97	93.33	89.77	90.69	91.27
MRELB $R^{riu2}_{r,p}$	93.52	83.91	84.68	87.37	94.95	88.59	89.05	90.86	95.83	89.72	91.16	92.24
ARELB $P^{riu2}_{r,p}$	99.61	98.61	98.84	99.02	99.74	99.35	99.44	99.51	99.84	99.14	99.79	99.59
ARELB $N^{riu2}_{r,p}$	87.68	79.10	79.81	82.20	86.90	82.69	81.76	83.78	87.55	83.63	84.70	85.30
ARELB $R^{riu2}_{r,p}$	95.70	88.96	88.68	91.11	98.46	92.18	92.64	94.43	96.28	90.53	91.20	92.67
LBP $r^{riu2}_{r,p}$ [6]	95.42	88.73	82.15	88.77	97.03	90.23	86.57	91.28	93.02	88.59	87.04	89.55
ELBP $r^{riu2}_{r,p}$ [10]	99.32	97.92	97.59	98.28	99.51	98.54	97.64	98.56	99.45	97.99	97.78	98.41
(r, p)	(1,8)+(3,16)				(1,8)+(3,16)+(5,24)				(1,8)+(3,16)+(5,24)+(7,24)			
Method	TC10	TC12		Mean	TC10	TC12		Mean	TC10	TC12		Mean
GRELB $P^{riu2}_{r,p}$	99.82	98.80	98.59	99.07	99.92	99.51	99.44	99.63	99.95	99.51	99.75	99.74
GRELB $N^{riu2}_{r,p}$	91.38	80.74	82.08	84.73	96.15	89.38	88.98	91.50	98.80	95.39	95.67	96.62
GRELB $R^{riu2}_{r,p}$	96.85	89.75	89.84	92.14	99.24	93.80	93.24	95.43	98.78	94.35	94.56	95.90
MRELB $P^{riu2}_{r,p}$	99.11	97.57	97.18	97.95	99.82	99.38	99.12	99.44	99.82	99.56	99.42	99.60
MRELB $N^{riu2}_{r,p}$	91.35	84.93	82.50	86.26	96.07	91.30	91.23	92.86	98.05	95.16	95.95	96.39
MRELB $R^{riu2}_{r,p}$	95.00	85.30	85.95	88.75	97.06	90.49	90.23	92.59	97.34	91.57	91.02	93.31
ARELB $P^{riu2}_{r,p}$	99.82	98.70	98.63	99.05	99.92	99.51	99.61	99.68	99.90	99.38	99.72	99.66
ARELB $N^{riu2}_{r,p}$	92.06	80.58	81.57	84.74	96.35	88.96	88.68	91.33	98.44	95.81	96.18	96.81
ARELB $R^{riu2}_{r,p}$	97.66	90.95	90.14	92.91	98.91	93.84	94.31	95.68	98.41	94.03	94.24	95.56
LBP $r^{riu2}_{r,p}$ [6]	96.95	90.83	84.72	90.84	98.33	91.00	86.57	91.97	99.40	92.69	89.42	93.84
ELBP $r^{riu2}_{r,p}$ [10]	99.40	97.82	96.92	98.05	99.48	97.73	95.60	97.60	99.48	97.52	94.95	97.32

TABLE IV

CLASSIFICATION SCORES (%) ON Outex_TC11n (GAUSSIAN NOISE), Outex_TC11b (GAUSSIAN BLUR), Outex_TC23n AND Outex_TC23b. PROPOSED RELBP IS OBTAINED BY $(1, 8) + (3, 8) + (5, 8) + (7, 8)$, $w_c = 3$ AND $w_r = (3, 3, 5, 7)$

Datasets	Gaussian Noise Robustness					Gaussian Blur Robustness				
	Outex_TC11n	Outex_TC23n	Outex_TC11b			Outex_TC23b				
Method	$\sigma = 5$	$\sigma = 5$	$\sigma = 0.5$	$\sigma = 0.75$	$\sigma = 1$	$\sigma = 0.5$	$\sigma = 0.75$	$\sigma = 1$	$\sigma = 0.5$	$\sigma = 0.75$
GRELB $P^{riu2}_{r,p}$	90.8	73.8	100.0	99.8	85.0	100.0	87.5	63.8		
MRELB $P^{riu2}_{r,p}$	87.7	66.4	100.0	99.8	87.5	100.0	94.4	69.5		
ARELB $P^{riu2}_{r,p}$	90.6	67.4	100.0	99.8	87.5	100.0	88.7	65.7		
Dataset	Salt-and-Pepper Noise Robustness									
Outex_TC11s (24 classes)										
Method	$\rho = 5\%$	$\rho = 10\%$	$\rho = 15\%$	$\rho = 20\%$	$\rho = 30\%$	$\rho = 5\%$	$\rho = 10\%$	$\rho = 15\%$	$\rho = 20\%$	$\rho = 30\%$
GRELB $P^{riu2}_{r,p}$	26.9	16.0	6.7	4.6	4.2	9.6	2.4	1.5	1.5	1.5
MRELB $P^{riu2}_{r,p}$	100.0	100.0	100.0	100.0	97.5	99.9	99.7	99.8	98.1	74.3
ARELB $P^{riu2}_{r,p}$	24.2	8.3	4.4	4.2	4.2	5.6	1.5	1.5	1.5	1.5
Dataset	Robustness to Random Corrupted Pixels									
Outex_TC11c (24 classes)										
Method	$v = 5\%$	$v = 10\%$	$v = 20\%$	$v = 30\%$	$v = 40\%$	$v = 5\%$	$v = 10\%$	$v = 20\%$	$v = 30\%$	$v = 40\%$
GRELB $P^{riu2}_{r,p}$	78.5	62.7	30.8	14.6	7.5	47.6	19.4	5.4	1.7	1.5
MRELB $P^{riu2}_{r,p}$	100.0	100.0	100.0	96.9	76.7	99.5	98.5	95.4	74.1	34.3
ARELB $P^{riu2}_{r,p}$	76.3	61.7	26.0	8.3	4.8	41.8	17.1	4.1	1.6	1.5

patches $w_r \times w_r$ associated with radius r . We refer to a multiscale sampling scheme for MRELB as a template, and we will examine the performance of MRELB under different template settings.

We present the nine templates settings and the corresponding results in Table V. The nine templates were chosen following the methods of BRISK [24] and FREAK [25]. Template 1 is the default, as was the parameter choice used in previous experiments.

In order to avoid aliasing effects when sampling the image, the patch size $w_r \times w_r$ associated with the median operator

is set to be proportional to radius r . Template 2, with a slight increase in radius over template 1, produces the highest classification score in noise-free situations and gives high classification accuracies in noisy situations. The larger scales have much to offer, since the more local sampling of Template 4 performs the worst; clearly there is a limit to the utility of nonlocal information, since template 5 at 8 scales does not offer any improvement.

Templates 6 through 9 assess the choice of parameter w_r . It is fairly clear from Table V that larger patches lead to improved noise robustness, but at a cost of reduced

TABLE V
PARAMETER EVALUATION (%); p IS ALWAYS 8

Tmpl.	w_c	r	w_r	TC10	TC12		Mean	TC11b ($\sigma = 1$)	TC11s ($\rho=30\%$)	TC23s ($\rho=30\%$)
					t84	horizon				
Tmpl.1	3	(1, 3, 5, 7)	(3, 3, 5, 7)	99.38	99.17	99.51	99.35	87.50	97.50	74.26
Tmpl.2	3	(2, 4, 6, 8)	(3, 5, 7, 9)	99.82	99.38	99.77	99.65	93.75	100.00	93.97
Tmpl.3	3	(1, 2, 4, 8)	(3, 3, 5, 9)	99.56	99.21	99.70	99.49	89.58	97.08	67.57
Tmpl.4	3	(1, 2, 3, 4)	(3, 3, 5, 9)	98.75	98.29	97.73	98.26	68.54	81.67	48.09
Tmpl.5	3	(1 ~ 8)	(3, 3, 5, 5, 7, 9)	99.22	99.17	99.24	99.21	90.00	98.75	80.07
Tmpl.6	3	(2, 4, 6, 8)	(3, 7, 11, 15)	99.77	98.59	99.33	99.23	95.00	100.00	94.63
Tmpl.7	5	(2, 4, 6, 8)	(7, 9, 11, 13)	97.92	95.12	96.06	96.37	94.17	99.79	96.47
Tmpl.8	3	(2, 4, 6, 8)	(5, 7, 9, 11)	98.80	98.40	98.47	98.56	94.17	100.00	93.90
Tmpl.9	3	(2, 4, 6, 8)	(5, 9, 13, 17)	98.07	97.04	97.50	97.54	94.58	100.00	94.49

TABLE VI

RESULTS (%) FOR EVALUATION OF DIFFERENT ENCODING METHODS WITH $w_c = 3$, $r = (2, 4, 6, 8)$, $p = (8, 8, 8, 8)$, $w_r = (3, 5, 7, 9)$

Method	TC10	TC12		Mean	TC11b ($\sigma = 1$)	TC11s ($\rho=30\%$)	TC23s ($\rho=30\%$)	Feat. Dim.
		t84	horizon					
MRELBP ^{riu2} _{r,p}	99.82	99.38	99.77	99.65	93.75	100.00	93.97	800
MRELBP ^{faith} _{r,p}	99.84	99.33	99.72	99.63	95.83	100.00	96.10	2048
MRELBP ^{ham} _{r,p}	98.96	98.43	98.84	98.74	95.83	99.79	95.07	968
MRELBP ^{count} _{r,p}	98.91	97.50	97.96	98.12	95.00	99.79	93.09	648
MRELBP ^{num} _{r,p}	99.87	99.49	99.75	99.70	95.83	100.00	96.32	1568
MRELBP ^{ri} _{r,p}	98.15	97.92	98.40	98.16	96.46	100.00	97.57	10368

performance in noise-free contexts. Furthermore using larger patches increases the algorithm's computational complexity. We would maintain that the results in Table V argue in favour of Template 2, which we will use in the remainder of our experiments.

4) *Encoding Methods:* Six different encoding strategies were discussed in Section III-B; the corresponding experimental results are listed in Table VI. All six methods show relatively similar performance, with slightly higher performance from MRELBP^{faith}, our proposed MRELBP^{num}, and MRELBP^{riu2}. Because of the rather higher dimensionality of *faith* over *num*, and the poorer performance of *riu2* in noisy settings, we have a preference for the *num* encoding, but will continue to test the *riu2* encoding for consistency with other proposed approaches.

D. Comparative Evaluation

In this section, to avoid tuning parameters and to preserve consistency, all results for the proposed MRELBP^{riu2} _{r,p} and MRELBP^{num} _{r,p} descriptor are obtained with the four-scale Template 2 from Table V).

1) *Results for Experiment #1:* Table VII compares the classification performance of the proposed MRELBP^{riu2} _{r,p} and MRELBP^{num} _{r,p} descriptor with those of fifteen recent state-of-the-art LBP variants on the three Outex benchmark test suites. We can observe that our MRELBP approach performs significantly and consistently better than all 15 methods in comparison. The striking performance of MRELBP clearly demonstrates that the concatenated joint distributions of the proposed MRELBP_CI, MRELBP_NI and MRELBP_RD codes and the novel sampling scheme turns out to be a very powerful representation of image texture, making effective use

TABLE VII
COMPARING THE CLASSIFICATION SCORES (%) ACHIEVED BY THE PROPOSED APPROACH WITH THOSE ACHIEVED BY RECENT STATE-OF-THE-ART TEXTURE CLASSIFICATION METHODS ON THE THREE OUTEX TEST SUITES. SCORES ARE AS ORIGINALLY REPORTED, EXCEPT THOSE MARKED (\diamond) WHICH ARE TAKEN FROM THE WORK BY GUO *et al.* [12] AND THOSE MARKED (*) WHICH ARE OBTAINED ACCORDING OUR OWN IMPLEMENTATION. FOR CLBP, LBPD AND PRICoLBP_g, WE USED THE CODES PROVIDED BY THE AUTHORS

Method	TC10	TC12		Mean	Reference	Feature Dimension
		t84	horizon			
MRELBP ^{riu2} _{r,p}	99.82	99.38	99.77	99.65	This Paper	800
MRELBP ^{num} _{r,p}	99.87	99.49	99.75	99.70	This Paper	800
LBPR ^{riu2} _{r,p} VAR _{r,p} [6]	97.7		87.3	86.4	TPAMI 2002	864
VZ-MR8 [53]	93.59(\diamond)	92.55(\diamond)	92.82(\diamond)	92.99(\diamond)	ICIV 2005	960
MBP ^{riu2} _{r,p} [16]	89.92		95.18	95.55	ICIAR 2007	108
FLBP ^{riu2} _{r,p} [18]	97.53(*)	90.32(*)	86.87(*)	91.57(*)	ICIAR 2008	60
VZ-Patch [41]	92.00(\diamond)	91.41(\diamond)	92.06(\diamond)	91.82(\diamond)	TPAMI 2009	960
CLBP ^{riu2} _[12]	99.14		95.18	95.55	TIP 2010	2200
LTP ^{riu2} _{r,p} [15]	98.54(*)	92.59(*)	89.17(*)	93.43(*)	TIP 2010	108
LBPV ^{riu2} _{r,p} GM _{PD2} ^{P/2-1} [46]	97.63		95.06	93.88	PR 2010	2211
CLBC [13]	98.96		95.37	94.72	TIP 2012	1990
dist(S+M) _{r,p} [34]	98.93(*)		97.0	96.5	PR 2012	2668
NTLBP ^{faith} _{r,p} [19]	99.24		96.18	94.28	PRL 2012	108
NRLBP ^{riu2} _{r,p} [21]	93.44		86.13	87.38	TIP 2013	30
MSJLBP [35]	96.67(*)	95.21(*)	95.74(*)	95.87(*)	BMVC 2013	3540
PRICoLBP _g [11]	94.48(*)	92.57(*)	92.50(*)	93.18(*)	TPAMI 2014	3540
COV-LBPD [22]	98.78(*)	95.72(*)	97.62(*)	97.37(*)	TIP 2014	289

TABLE VIII
COMPARING THE CLASSIFICATION SCORES (%) ACHIEVED BY THE PROPOSED APPROACH WITH THOSE ACHIEVED BY RECENT STATE-OF-THE-ART TEXTURE CLASSIFICATION METHODS ON THE THREE OUTEX_TC36 TEST SUITES

Method	Outex_TC36	
	t84	horizon
MRELBP ^{riu2} _{r,p}	92.49	91.55
MRELBP ^{num} _{r,p}	92.55	91.50
LBPR ^{riu2} _{r,p} [6]	85.56	83.98
ELBP ^{riu2} _{r,p} [10]	88.89	88.13
CLBP ^{riu2} _{r,p} [12]	86.67	87.62
MBP ^{riu2} _{r,p} [16]	54.81	54.37
NTLBP ^{faith} _{r,p} [19]	76.67	73.05
PRICoLBP _g [11]	77.39	76.47
LTP ^{riu2} _{r,p} [15]	75.28	75.48
MSJLBP [35]	76.21	75.97
COV-LBPD [22]	80.57	83.47

of both micro- and macrostructures. To the best of our knowledge, the near perfect classification scores of 99.87%, 99.49% and 99.77% for our proposed approach are the best reported for Outex_TC10, Outex_TC12_000 and Outex_TC12_001. Keeping in mind the variations in gray scale and rotation present in the three test suites, the results in Table VII firmly demonstrate the gray-scale and rotation invariance claimed of the MRELBP approach. Table VII also compares the feature dimensionality of the methods, where we can observe the modest feature dimensionality of the proposed approach, with corresponding savings in computational time and memory storage.

Table VIII tests the performance of our proposed descriptors on the more challenging test suites Outex_TC36_000

TABLE IX

CLASSIFICATION SCORES (%) FOR VARIOUS METHODS ON Outex_TC11n, Outex_TC11b, Outex_TC23n AND Outex_TC23b.
ALL RESULTS (INCLUDING RESULTS IN TABLES X, XI AND XII) ARE OBTAINED WITH A NNC CLASSIFIER

Robust to	Gaussian Noise		Gaussian Blur								
	Datasets	Outex_TC11n	Outex_TC23n	Outex_TC11b				Outex_TC23b			
Method				$\sigma=0.5$	$\sigma=0.75$	$\sigma=1$	$\sigma=1.25$	$\sigma=0.5$	$\sigma=0.75$	$\sigma=1$	$\sigma=1.25$
MRELBP ^{riu2} _{r,p}	91.5	79.2	100.0	100.0	93.8	75.4	99.9	97.9	85.8	61.8	
MRELBP ^{nun} _{r,p}	91.5	80.1	100.0	100.0	95.8	78.3	99.9	98.8	89.4	67.4	
LBP ^{riu2} [6]	12.7	5.7	89.0	45.4	22.5	12.1	66.1	28.7	15.8	10.8	
ELBP ^{riu2} _{r,p} [10]	12.3	6.0	100.0	72.7	40.8	17.7	93.8	51.5	29.0	15.7	
CLLBP ^{riu2} _{r,p} [12]	13.5	9.0	99.8	81.7	52.9	24.0	89.3	64.9	44.8	28.1	
MBP ^{riu2} _{r,p} [16]	11.7	5.1	67.9	18.8	12.7	8.3	50.1	16.9	9.6	8.4	
NTLBP ^{faith} _{r,p} [19]	15.6	5.2	82.1	39.0	26.0	17.3	56.3	22.9	14.0	8.3	
PRICoLBP _g [11]	15.4	5.6	98.1	50.0	26.5	14.4	81.1	32.5	19.6	11.3	
LTP ^{riu2} _{r,p} [15]	8.5	3.5	88.3	37.7	17.7	8.8	61.0	30.0	16.3	9.9	
NRLBP ^{riu2} _{r,p} [21]	11.7	3.8	85.4	29.4	14.2	9.4	55.9	23.6	12.1	7.1	
MSJLBP [35]	17.7	4.9	96.0	46.0	26.0	11.9	74.9	28.9	14.8	8.9	
dis(S+M) _{r,p} [34]	15.8	5.9	97.1	62.3	35.6	19.6	78.8	34.8	19.6	11.1	
COV-LBPD [22]	23.5	13.2	99.2	86.9	65.6	46.0	86.9	56.0	40.0	31.0	

TABLE X

CLASSIFICATION SCORES (%) FOR VARIOUS METHODS ON Outex_TC11s AND Outex_TC23s

Dataset	Salt-and-Pepper Noise Robustness													
	Outex_TC11s (24 classes)						Outex_TC23s (68 classes)							
Method	$\rho=5\%$	$\rho=10\%$	$\rho=15\%$	$\rho=20\%$	$\rho=30\%$	$\rho=40\%$	$\rho=50\%$	$\rho=5\%$	$\rho=10\%$	$\rho=15\%$	$\rho=20\%$	$\rho=30\%$	$\rho=40\%$	$\rho=50\%$
MRELBP ^{riu2} _{r,p}	100.0	100.0	100.0	100.0	100.0	85.8	50.2	100.0	99.9	99.9	99.1	94.0	54.6	19.2
MRELBP ^{nun} _{r,p}	100.0	100.0	100.0	100.0	100.0	92.9	60.0	100.0	99.9	99.9	99.3	96.3	69.3	26.2
LBP ^{riu2} _{r,p} [6]	38.5	4.4	4.2	4.2	4.2	4.2	4.2	15.3	6.3	2.7	1.6	2.9	1.8	1.5
ELBP ^{riu2} _{r,p} [10]	31.9	10.4	6.7	4.2	4.2	4.2	4.2	14.0	4.3	2.6	1.5	1.5	1.5	1.5
CLLBP ^{riu2} [12]	10.6	7.7	7.9	8.3	4.2	4.2	4.2	7.6	2.9	1.5	1.5	1.5	1.5	1.5
MBP ^{riu2} _{r,p} [16]	29.6	11.7	8.3	6.9	4.2	4.2	4.2	14.6	4.3	2.6	1.7	1.5	1.5	1.5
NTLBP ^{faith} _{r,p} [19]	53.3	27.5	13.5	11.3	5.4	4.2	4.2	28.2	9.9	7.4	6.1	1.7	1.5	1.5
PRICoLBP _g [11]	9.6	8.1	5.2	4.2	4.2	4.2	4.2	4.2	3.0	2.1	1.5	1.5	1.5	1.5
LTP ^{riu2} _{r,p} [15]	10.2	4.2	4.2	6.5	8.3	4.2	4.2	1.7	2.5	2.9	1.5	2.9	1.5	1.5
NRLBP ^{riu2} _{r,p} [21]	5.8	5.8	4.2	4.2	5.2	5.6	4.2	1.7	1.5	1.5	0.1	1.5	1.5	2.1
MSJLBP [35]	14.2	10.2	8.3	8.3	4.4	4.2	4.2	7.1	4.7	3.5	2.4	1.5	1.5	1.5
dis(S+M) _{r,p} [34]	18.5	4.4	5.8	8.3	4.2	4.2	4.2	7.7	3.0	4.3	4.4	2.0	1.5	1.9
COV-LBPD [22]	27.1	13.8	8.3	7.7	4.2	4.2	4.2	10.7	4.5	2.9	3.0	1.5	1.5	1.2

TABLE XI

CLASSIFICATION SCORES (%) FOR VARIOUS METHODS ON Outex_TC11c AND Outex_TC23c

Dataset	Robustness to Random Corrupted Pixels											
	Outex_TC11c (24 classes)						Outex_TC23c (68 classes)					
Method	$v=5\%$	$v=10\%$	$v=20\%$	$v=30\%$	$v=40\%$	$v=5\%$	$v=10\%$	$v=20\%$	$v=30\%$	$v=40\%$		
MRELBP ^{riu2} _{r,p}	100.0	100.0	100.0	99.6	90.6	99.6	99.2	96.9	89.8	57.5		
MRELBP ^{nun} _{r,p}	100.0	100.0	100.0	100.0	93.3	99.4	99.3	97.7	92.8	65.7		
LBP ^{riu2} _{r,p} [6]	53.1	9.8	4.2	4.2	4.2	4.2	24.5	5.7	1.5	1.5	1.5	
ELBP ^{riu2} _{r,p} [10]	66.7	30.8	12.3	6.0	4.2	4.2	26.0	7.6	3.8	3.2	2.4	
CLLBP ^{riu2} [12]	72.7	29.2	4.2	4.2	4.2	4.2	38.9	6.2	2.3	2.1	1.8	
MBP ^{riu2} _{r,p} [16]	39.8	17.1	8.3	4.8	4.2	4.2	19.9	7.6	2.0	1.5	1.5	
NTLBP ^{faith} _{r,p} [19]	64.4	36.0	8.3	8.3	8.3	8.3	39.4	14.0	5.6	3.7	2.9	
PRICoLBP _g [11]	31.7	10.0	4.2	4.2	4.2	4.2	9.0	3.0	1.5	1.5	1.5	
LTP ^{riu2} _{r,p} [15]	49.0	17.5	8.1	4.2	4.2	4.2	15.8	6.0	4.1	4.0	1.5	
NRLBP ^{riu2} _{r,p} [21]	50.8	29.0	16.7	11.7	4.2	4.2	15.4	7.4	3.8	1.5	1.9	
MSJLBP [35]	32.3	16.7	7.5	4.2	4.2	4.2	14.4	5.6	2.7	1.7	1.2	
dis(S+M) _{r,p} [34]	45.0	18.5	4.2	4.2	4.2	4.2	15.9	4.5	3.1	2.9	1.5	
COV-LBPD [22]	26.9	17.7	8.5	4.6	4.2	4.2	13.0	7.1	3.2	1.8	1.5	

and Outex_TC36_001, which have 108 texture classes. We can observe that our proposed MRELBP descriptors outperform all other state of the art methods.

2) *Results for Experiment #2:* We conducted extensive experiments to test the noise robustness of our approach, using the test suites we described in Section IV-A. The test results are shown in Tables IX, X, and XI. The results are all consistently strong: the proposed MRELBP descriptors have exceptional noise tolerance that could not be matched by any of the state of the art LBP variants. There are difficult

noise levels where the proposed approach still offers strong performance, but where not a single state-of-the-art method delivers acceptable results.

Finally, Table XII illustrates the effect of introducing a median preprocessing filter, contrasting results with and without preprocessing. It is clearly observed that our proposed MRELBP outperforms all other LBP variants consistently and significantly, no matter with or without preprocessing. The results in Table XII show that preprocessing (with a median filter here) does not necessarily improve the noise robustness.

TABLE XII

COMPARING THE CLASSIFICATION SCORES (%) OF LBP VARIANTS AGAINST DIFFERENT NOISE TYPES IN TWO SITUATIONS: WITH OR WITHOUT PREPROCESSING WITH A MEDIAN FILTERING APPROACH

PreProcessing	None				Median Filtering				
	Outex_	TC11n		TC11b		TC11s		TC11c	
		$\sigma = 5\%$	$\rho = 1\%$	$\sigma = 5\%$	$\rho = 50\%$	$\sigma = 5\%$	$\rho = 50\%$	$\sigma = 5\%$	$\rho = 50\%$
MRELBP ^{r+u2} (Ours)	91.46	93.75	50.21	59.79	92.92	78.96	85.42	67.71	
LBP ^{r+u2} _{r,p} [6]	12.71	22.50	4.17	4.17	46.25	12.92	24.17	12.92	
ELBP ^{r+u2} _{r,p} [10]	12.29	40.83	4.17	4.17	63.13	18.33	15.21	12.92	
CLBP ^{r+u2} _{r,p} [12]	13.54	52.92	4.17	4.17	63.13	22.50	10.42	13.54	
MBP ^{r+u2} _{r,p} [16]	11.67	12.71	4.17	4.17	16.67	8.33	13.96	11.25	
NTLBP ^{faith} _{r,p} [19]	15.63	26.04	4.17	8.13	34.79	17.92	13.96	11.25	
PRICoLBP _g [11]	15.42	26.46	4.17	4.17	40.00	9.17	5.21	5.83	
LTP ^{r+u2} _{r,p} [15]	8.54	17.71	4.17	4.17	25.63	8.54	10.83	13.75	
NRLBP ^{r+u2} _{r,p} [21]	11.67	14.17	4.17	4.17	29.38	8.54	4.38	17.92	
MSJLBP [35]	17.71	26.04	4.17	4.17	36.25	8.54	13.75	8.75	
dis(S+M) _{r,p} [34]	15.83	35.63	4.17	4.17	40.63	17.08	12.92	9.38	
COV-LBDP [22]	23.54	65.63	4.17	4.17	41.46	30.83	12.29	12.29	

TABLE XIII

COMPARING THE CLASSIFICATION SCORES (%) ACHIEVED BY THE PROPOSED APPROACH WITH THOSE ACHIEVED BY RECENT STATE-OF-THE-ART METHODS ON THE KTHTIPS2b DATABASE. ALL SCORES ARE OBTAINED WITH NNC CLASSIFICATION, UNLESS OTHERWISE STATED

Method	Accuracy (%)
MRELBP ^{r+u2} (SVM)	77.91%
MRELBP ^{r+u2} (SVM)	77.34%
MRELBP ^{r+u2}	68.98
MRELBP ^{r+u2}	69.13
LBP ^{r+u2} [6]	60.35
ELBP ^{r+u2} [10]	64.84
CLBP ^{r+u2} [12]	63.87
MBP ^{r+u2} [16]	60.29
NTLBP ^{faith} _{r,p} [19]	58.78
PRICoLBP _g [11]	61.17
LTP ^{r+u2} _{r,p} [15]	62.12
NRLBP ^{r+u2} _{r,p} [21]	57.00
MSJLBP [35]	65.51
COV-LBDP [22]	63.47
MWLD [56]	64.7
VZ-MR8 [53]	55.7
VZ-Patch [41]	60.7

For instance, preprocessing always decreases the performance in the case of Gaussian blur. Therefore, the noise robustness inherent in our proposed MRELBP is clearly an attractive advantage.

Results in Table XII further confirm the noise robustness of the proposed MRELBP, emphasizing that no pre-smoothing is necessary. The absence of spatial smoothing is a significant advantage for MRELBP, as local spatial information is important for texture recognition, whereas pre-smoothing can suppress important local texture information, a serious drawback for texture recognition in low-noise situations.

3) *Results for Experiment #3:* A final experiment tests the generalizability of MRELBP to textures other than those present in the Outex database. The datasets we tested include CUReT, UMD, KTHTIPS2b and ALOT, discussed in Section IV-A, with results shown in Tables XIII (KTHTIPS2b), XV (CUReT), XIV (UMD) and XVI (ALOT).

The CUReT database has only small rotation variations, whereas our proposed MRELBP has a strong rotation invariance property, nevertheless from Table XV we can see that the proposed MRELBP with SVM produces the highest classification score on CUReT despite the fact that we have no pretraining step, in contrast to [39]–[41], [43], and [53].

TABLE XIV

COMPARING THE CLASSIFICATION SCORES (%) ACHIEVED BY THE PROPOSED APPROACH WITH THOSE ACHIEVED BY RECENT STATE-OF-THE-ART METHODS ON THE UMD DATABASE

Classifier	Method	Accuracy (%)
NNC	MRELBP ^{r+u2} _{r,p}	98.66
NNC	MRELBP ^{r+u2} _{r,p}	98.64
SVM	MRELBP ^{r+u2} _{r,p}	99.36
SVM	MRELBP ^{r+u2} _{r,p}	99.41
NNC	LBP ^{r+u2} _{r,p} [6]	95.85
	ELBP [10]	98.93
	CLBP [12]	98.32
	MBP ^{r+u2} [16]	93.09
	NTLBP ^{faith} _{r,p} [19]	95.32
	PRICoLBP _g [11]	95.69
	LTP ^{r+u2} [15]	96.55
	NRLBP ^{r+u2} [21]	93.21
	MSJLBP [35]	96.53
	COV-LBDP [22]	92.99
SVM	Xu-OTF [49]	98.49
	Xu-WMFS [49]	98.68

TABLE XV

COMPARING THE SCORES (%) ACHIEVED BY THE PROPOSED APPROACH WITH THOSE ACHIEVED BY RECENT STATE OF THE ART METHODS ON THE CUReT DATABASE. SCORES ARE AS ORIGINALLY REPORTED, EXCEPT (*) FROM [40]

Classifier	Method	Accuracy (%)	Published in
SVM	MRELBP ^{r+u2} _{r,p}	99.02	This paper
NNC	MRELBP ^{r+u2} _{r,p}	97.10	This paper
NNC	CLBP_CSM [12]	97.39	TIP 2010
	CLBP_CSM [13]	95.39	TIP 2012
	LBP ^{v2} _{v2} GM ^{p2,l} [46]	96.04	PR 2010
	dis(S+M) _{r,p} [34]	98.3	PR 2012
	VZ-MR8 [53]	97.43	IJCV 2005
	VZ-Patch [41]	98.03	TPAMI 2009
	Lazebnik <i>et al.</i> [39]	72.5(*)	TPAMI 2005
	MultiScale BIF [42]	98.6	IJCV 2010
	RP [43]	98.52	TPAMI 2012
	Hayman <i>et al.</i> [57]	98.46	IMAVIS 2010
SVM	Zhang <i>et al.</i> [40]	95.3	IJCV 2007

TABLE XVI

COMPARING THE CLASSIFICATION SCORES (%) OF VARIOUS LBP VARIANTS ON THE ALOT DATABASE. ALL RESULTS ARE OBTAINED WITH A NNC CLASSIFIER

Method	Accuracy (%)
MRELBP ^{r+u2} _{r,p}	97.28%
LBP ^{r+u2} _{r,p} [6]	92.16
ELBP ^{r+u2} [10]	97.21
CLBP ^{r+u2} _{r,p} [12]	96.66
MBP ^{r+u2} [16]	85.10
NTLBP ^{faith} _{r,p} [19]	92.00
PRICoLBP _g [11]	94.38
LTP ^{r+u2} _{r,p} [15]	91.43
NRLBP ^{r+u2} _{r,p} [21]	85.20
MSJLBP [35]	95.65
COV-LBDP [22]	92.82

Table XIV lists the results on the UMD database, which contains significant variations in scale and rotation. We can observe that our MRELBP performs very well, producing the highest score. Similarly the results in Table XIII reveal that MRELBP significantly outperforms many state of the art methods on the difficult KTHTIPS2b database. Finally, the results on the large scale ALOT dataset, listed in XVI, demonstrate that MRELBP performs the best. We would like to mention that a recent LBP based approach named Pattern Fractal Spectrum (PFS) proposed by Quan *et al.* [55] gives 97.5% classification accuracy with RBF kernel SVM classifier on ALOT. Our MRELBP can produce 99.08% on ALOT with SVM classifier.

Finally, the proposed MRELBP descriptor has a modest computational cost. In comparison with the traditional multiscale LBP_{r,p}^{riu2}, our MRELBP is somewhat slower. However, the computational complexity of MRELBP is much lower than many existing LBP variants. As a matter of fact, in the feature extraction stage MRELBP has a similar computational cost as traditional multiscale LBP, except for the computation of local medians in MRELBP, which is fast, however in practice we use fewer neighbors for MRELBP than in many other LBP variants. In the classification stage, the feature dimensionality of MRELBP (800) is moderate compared with various LBP variants, so MRELBP is efficient as a texture descriptor.

V. CONCLUSIONS

We have presented a novel MRELBP descriptor to enhance the performance of current LBP variants. It outperforms recent state of the art LBP type descriptors in noise free situations and demonstrates striking robustness to image noise including Gaussian white noise, Gaussian blur, Salt-and-Pepper and pixel corruption. The proposed MRELBP has attractive properties of strong discriminativeness, gray scale and rotation invariance, no need for a pretraining, no tuning of parameters, and computational efficiency. As future work, we wish to investigate high-level applications such as image patching and object recognition.

REFERENCES

- [1] M. Pietikäinen, A. Hadid, G. Zhao, and T. Ahonen, *Computer Vision Using Local Binary Patterns*. London, U.K.: Springer, 2011.
- [2] M. Pietikäinen and G. Zhao, “Two decades of local binary patterns: A survey,” in *Advances in Independent Component Analysis and Learning Machines*. Amsterdam, The Netherlands: Elsevier, 2015.
- [3] U. Kandaswamy, S. A. Schuckers, and D. Adjeroh, “Comparison of texture analysis schemes under nonideal conditions,” *IEEE Trans. Image Process.*, vol. 20, no. 8, pp. 2260–2275, Aug. 2011.
- [4] J. Zhang, M. Marszalek, S. Lazebnik, and C. Schmid, “Local features and kernels for classification of texture and object categories: A comprehensive study,” *Int. J. Comput. Vis.*, vol. 73, no. 2, pp. 213–238, Jun. 2007.
- [5] S. Brahnam, L. C. Jain, L. Nanni, and A. Lumini, Eds., *Local Binary Patterns: New Variants and Applications*. London, U.K.: Springer, 2014.
- [6] T. Ojala, M. Pietikäinen, and T. Maenpää, “Multiresolution gray-scale and rotation invariant texture classification with local binary patterns,” *IEEE Trans. Pattern Anal. Mach. Intell.*, vol. 24, no. 7, pp. 971–987, Jul. 2002.
- [7] T. Ahonen, A. Hadid, and M. Pietikäinen, “Face description with local binary patterns: Application to face recognition,” *IEEE Trans. Pattern Anal. Mach. Intell.*, vol. 28, no. 12, pp. 2037–2041, Dec. 2006.
- [8] G. Zhao and M. Pietikäinen, “Dynamic texture recognition using local binary patterns with an application to facial expressions,” *IEEE Trans. Pattern Anal. Mach. Intell.*, vol. 29, no. 6, pp. 915–928, Jun. 2007.
- [9] T. Ahonen, J. Matas, C. He, and M. Pietikäinen, “Rotation invariant image description with local binary pattern histogram Fourier features,” in *Proc. Scandinavian Conf. Image Anal.*, 2009, pp. 61–70.
- [10] L. Liu, L. Zhao, Y. Long, G. Kuang, and P. Fieguth, “Extended local binary patterns for texture classification,” *Image Vis. Comput.*, vol. 30, no. 2, pp. 86–99, Feb. 2012.
- [11] X. Qi, R. Xiao, C.-G. Li, Y. Qiao, J. Guo, and X. Tang, “Pairwise rotation invariant co-occurrence local binary pattern,” *IEEE Trans. Pattern Anal. Mach. Intell.*, vol. 36, no. 11, pp. 2199–2213, Nov. 2014.
- [12] Z. Guo, L. Zhang, and D. Zhang, “A completed modeling of local binary pattern operator for texture classification,” *IEEE Trans. Image Process.*, vol. 19, no. 6, pp. 1657–1663, Jun. 2010.
- [13] Y. Zhao, D.-S. Huang, and W. Jia, “Completed local binary count for rotation invariant texture classification,” *IEEE Trans. Image Process.*, vol. 21, no. 10, pp. 4492–4497, Oct. 2012.
- [14] S. Liao, M. W. K. Law, and A. Chung, “Dominant local binary patterns for texture classification,” *IEEE Trans. Image Process.*, vol. 18, no. 5, pp. 1107–1118, May 2009.
- [15] X. Tan and B. Triggs, “Enhanced local texture feature sets for face recognition under difficult lighting conditions,” *IEEE Trans. Image Process.*, vol. 19, no. 6, pp. 1635–1650, Jun. 2010.
- [16] A. Hafiane, G. Seetharaman, and B. Zavidovique, “Median binary pattern for textures classification,” in *Proc. 4th Int. Conf. Image Anal. Recognit.*, 2007, pp. 387–398.
- [17] V. Ojansivu, E. Rahtu, and J. Heikkilä, “Rotation invariant local phase quantization for blur insensitive texture analysis,” in *Proc. IEEE Int. Conf. Pattern Recognit. (ICPR)*, Dec. 2008, pp. 1–4.
- [18] D. K. Iakovovidis, E. G. Keramidas, and D. Maroulis, “Fuzzy local binary patterns for ultrasound texture characterization,” in *Image Analysis and Recognition* (Lecture Notes in Computer Science), A. Campilho and M. Kamel, Eds. Berlin, Germany: Springer, 2008, pp. 750–759.
- [19] A. Fathi and A. R. Naghsh-Nilchi, “Noise tolerant local binary pattern operator for efficient texture analysis,” *Pattern Recognit. Lett.*, vol. 33, no. 9, pp. 1093–1100, Jul. 2012.
- [20] J. Chen, V. Kellokumpu, G. Zhao, and M. Pietikäinen, “RLBP: Robust local binary pattern,” in *Proc. Brit. Vis. Conf. Comput. Vis. (BMVC)*, 2013, pp. 1–10.
- [21] J. Ren, X. Jiang, and J. Yuan, “Noise-resistant local binary pattern with an embedded error-correction mechanism,” *IEEE Trans. Image Process.*, vol. 22, no. 10, pp. 4049–4060, Oct. 2013.
- [22] X. Hong, G. Zhao, M. Pietikäinen, and X. Chen, “Combining LBP difference and feature correlation for texture description,” *IEEE Trans. Image Process.*, vol. 23, no. 6, pp. 2557–2568, Jun. 2014.
- [23] E. Tola, V. Lepetit, and P. Fua, “DAISY: An efficient dense descriptor applied to wide-baseline stereo,” *IEEE Trans. Pattern Anal. Mach. Intell.*, vol. 32, no. 5, pp. 815–830, May 2010.
- [24] S. Leutenegger, M. Chli, and R. Y. Siegwart, “BRISK: Binary Robust invariant scalable keypoints,” in *Proc. Int. Conf. Comput. Vis. (ICCV)*, Nov. 2011, pp. 2548–2555.
- [25] A. Alahi, R. Ortiz, and P. Vandergheynst, “FREAK: Fast retina keypoint,” in *Proc. Comput. Vis. Pattern Recognit. (CVPR)*, Jun. 2012, pp. 510–517.
- [26] L. Liu, P. Fieguth, M. Pietikäinen, and S. Lao, “Median robust extended local binary pattern for texture classification,” in *Proc. IEEE Int. Conf. Image Process.*, Sep. 2015, pp. 2319–2323.
- [27] A. Fernández, M. X. Álvarez, and F. Bianconi, “Texture description through histograms of equivalent patterns,” *J. Math. Imag. Vis.*, vol. 45, no. 1, pp. 76–102, Jan. 2013.
- [28] D. Huang, C. Shan, M. Ardabiliyan, Y. Wang, and L. Chen, “Local binary patterns and its application to facial image analysis: A survey,” *IEEE Trans. Syst., Man, Cybern. C, Appl. Rev.*, vol. 41, no. 6, pp. 765–781, Nov. 2011.
- [29] S. A. O. Vargas, F. Rooms, and W. Philips, “Geometric local binary patterns a new approach to analyse texture in images,” in *Proc. Int. Conf. Topol. Appl.*, 2010, pp. 179–181.
- [30] L. Nanni, A. Lumini, and S. Brahnam, “Local binary patterns variants as texture descriptors for medical image analysis,” *Artif. Intell. Med.*, vol. 49, no. 2, pp. 117–125, Jun. 2010.
- [31] S. U. Hussain and B. Triggs, “Visual recognition using local quantized patterns,” in *Proc. Eur. Conf. Comput. Vis. (ECCV)*, 2012, pp. 716–729.
- [32] L. Wolf, T. Hassner, and Y. Taigman, “Effective unconstrained face recognition by combining multiple descriptors and learned background statistics,” *IEEE Trans. Pattern Anal. Mach. Intell.*, vol. 33, no. 10, pp. 1978–1990, Oct. 2011.
- [33] H. Yang and Y. Wang, “A LBP-based face recognition method with hamming distance constraint,” in *Proc. Int. Conf. Image Graph.*, Aug. 2007, pp. 645–649.
- [34] Y. Guo, G. Zhao, and M. Pietikäinen, “Discriminative features for texture description,” *Pattern Recognit.*, vol. 45, no. 10, pp. 3834–3843, Oct. 2012.
- [35] X. Qi, Y. Qiao, C. Li, and J. J. Guo, “Multi-scale joint encoding of local binary patterns for texture and material classification,” in *Proc. Brit. Mach. Vis. Conf. (BMVC)*, Sep. 2013, pp. 1–11.
- [36] K. Wang, C.-E. Bichot, C. Zhu, and B. Li, “Pixel to patch sampling structure and local neighboring intensity relationship patterns for texture classification,” *IEEE Signal Process. Lett.*, vol. 20, no. 9, pp. 853–856, Sep. 2013.
- [37] T. Ahonen and M. Pietikäinen, “Soft histograms for local binary patterns,” in *Proc. Finnish Signal Process. Symp.*, 2007, pp. 645–649.
- [38] M. Calonder, V. Lepetit, M. Ozuysal, T. Trzcinski, C. Strecha, and P. Fua, “BRIEF: Computing a local binary descriptor very fast,” *IEEE Trans. Pattern Anal. Mach. Intell.*, vol. 34, no. 7, pp. 1281–1298, Jul. 2012.

- [39] S. Lazebnik, C. Schmid, and J. Ponce, "A sparse texture representation using local affine regions," *IEEE Trans. Pattern Anal. Mach. Intell.*, vol. 27, no. 8, pp. 1265–1278, Aug. 2005.
- [40] B. Zhang, S. Shan, X. Chen, and W. Gao, "Histogram of Gabor phase patterns (HGPP): A novel object representation approach for face recognition," *IEEE Trans. Image Process.*, vol. 16, no. 1, pp. 57–68, Jan. 2007.
- [41] M. Varma and A. Zisserman, "A statistical approach to material classification using image patch exemplars," *IEEE Trans. Pattern Anal. Mach. Intell.*, vol. 31, no. 11, pp. 2032–2047, Nov. 2009.
- [42] M. Crosier and L. D. Griffin, "Using basic image features for texture classification," *Int. J. Comput. Vis.*, vol. 88, no. 3, pp. 447–460, Jul. 2010.
- [43] L. Liu and P. W. Fieguth, "Texture classification from random features," *IEEE Trans. Pattern Anal. Mach. Intell.*, vol. 34, no. 3, pp. 574–586, Mar. 2012.
- [44] F. Bianconi and A. Fernández, "On the occurrence probability of local binary patterns: A theoretical study," *J. Math. Imag. Vis.*, vol. 40, no. 3, pp. 259–268, Jul. 2014.
- [45] H. Zhou, R. Wang, and C. Wang, "A novel extended local-binary-pattern operator for texture analysis," *Inf. Sci.*, vol. 178, no. 22, pp. 4314–4325, Nov. 2008.
- [46] Z. Guo, L. Zhang, and D. Zhang, "Rotation invariant texture classification using LBP variance (LBPV) with global matching," *Pattern Recognit.*, vol. 43, no. 3, pp. 706–719, Mar. 2010.
- [47] C.-C. Chang and C.-J. Lin, *Library for Support Vector Machines*. [Online]. Available: <http://www.csie.ntu.edu.tw/cjlin/libsvm>, accessed Dec. 2014.
- [48] T. Ojala, T. Mäenpää, M. Pietikäinen, J. Viertola, and S. Huovinen, "Outex—New framework for empirical evaluation of texture analysis algorithms," in *Proc. 16th Int. Conf. Pattern Recognit.*, 2002, pp. 701–706.
- [49] Y. Xu, X. Yang, H. Ling, and H. Ji, "A new texture descriptor using multifractal analysis in multi-orientation wavelet pyramid," in *Proc. IEEE Conf. Comput. Vis. Pattern Recognit. (CVPR)*, Jun. 2010, pp. 161–168.
- [50] P. Mallikarjuna, M. Fritz, A. Targhi, E. Hayman, B. Caputo, and J.-O. Eklundh, *The KTH-Tips and KTH-Tips2 Databases*. [Online]. Available: <http://www.nada.kth.se/cvap/databases/kth-tips/>, accessed Sep. 2014.
- [51] G. J. Burghouts and J.-M. Geusebroek, "Material-specific adaptation of color invariant features," *Pattern Recognit. Lett.*, vol. 30, no. 3, pp. 306–313, Feb. 2009.
- [52] J. Wright, A. Y. Yang, A. Ganesh, S. S. Sastry, and Y. Ma, "Robust face recognition via sparse representation," *IEEE Trans. Pattern Anal. Mach. Intell.*, vol. 31, no. 2, pp. 210–227, Feb. 2009.
- [53] M. Varma and A. Zisserman, "A statistical approach to texture classification from single images," *Int. J. Comput. Vis.*, vol. 62, no. 1, pp. 61–81, Apr. 2005.
- [54] B. Caputo, E. Hayman, and P. Mallikarjuna, "Class-specific material categorisation," in *Proc. Int. Conf. Comput. Vis. (ICCV)*, 2005, pp. 1597–1604.
- [55] Y. Quan, Y. Xu, and Y. Sun, "A distinct and compact texture descriptor," *Image Vis. Comput.*, vol. 32, no. 4, pp. 250–259, Apr. 2014.
- [56] J. Chen *et al.*, "WLD: A robust local image descriptor," *IEEE Trans. Pattern Anal. Mach. Intell.*, vol. 32, no. 9, pp. 1705–1720, Sep. 2010.
- [57] B. Caputo, E. Hayman, M. Fritz, and J.-O. Eklundh, "Classifying materials in the real world," *Image Vis. Comput.*, vol. 28, no. 1, pp. 150–163, Jan. 2010.



Li Liu received the B.S. degree in communication engineering, the M.S. degree in photogrammetry and remote sensing, and the Ph.D. degree in information and communication engineering from the National University of Defense Technology (NUDT), Changsha, China, in 2003, 2005, and 2012, respectively. She joined as a Faculty Member with NUDT in 2012, where she is currently an Assistant Professor with the School of Information System and Management. During her Ph.D. study, she spent two years and three months as a Visiting Student with the University of Waterloo, Canada, from 2008 to 2010. She visited the Multimedia Laboratory, Chinese University of Hong Kong, as a Visiting Scholar from 2015 to 2016. Her current research interests include computer vision, texture analysis, pattern recognition, and object detection.



Songyang Lao received the B.S. degree in information system engineering and the Ph.D. degree in system engineering from the National University of Defense Technology, Changsha, China, in 1990 and 1996, respectively. He joined as a Faculty Member with the National University of Defense Technology, in 1996, where he is currently a Professor with the School of Information System and Management. He was a Visiting Scholar with Dublin City University, Irish, from 2004 to 2005. His current research interests include image processing and video analysis and human-computer interaction.



Paul W. Fieguth (S'87–M'96–SM'11) received the B.A.Sc. degree in electrical engineering from the University of Waterloo, ON, Canada, in 1991, and the Ph.D. degree in electrical engineering from the Massachusetts Institute of Technology, Cambridge, in 1995.

He joined as a Faculty Member with the University of Waterloo in 1996, where he is currently a Professor of Systems Design Engineering. He has held visiting appointments with the University of Heidelberg, Germany, INRIA/Sophia, France, the

Cambridge Research Laboratory, Boston, Oxford University, and the Rutherford Appleton Laboratory, U.K., and post-doctoral positions in Computer Science with the University of Toronto and in Information and Decision Systems with MIT. His research interests include statistical signal and image processing, hierarchical algorithms, data fusion, and the interdisciplinary applications of such methods, particularly to remote sensing.



3D face recognition, 3D modeling, pattern recognition, and signal processing.



Xiaogang Wang received the B.S. degree from the University of Science and Technology of China, in 2001, the M.S. degree from the Chinese University of Hong Kong, in 2003, and the Ph.D. degree from the Computer Science and Artificial Intelligence Laboratory, Massachusetts Institute of Technology, in 2009. He is currently an Associate Professor with the Department of Electronic Engineering, The Chinese University of Hong Kong. His research interests include computer vision and machine learning.



Matti Pietikäinen (F'12) received the D.Sc. degree in technology from the University of Oulu, Finland. He is currently a Professor, the Scientific Director of Infotech Oulu, and the Director of the Center for Machine Vision Research with the University of Oulu. From 1980 to 1981 and from 1984 to 1985, he visited the Computer Vision Laboratory, University of Maryland. He has made pioneering contributions, e.g., to local binary pattern methodology, texture-based image and video analysis, and facial image analysis. He has authored over 285 refereed papers in international journals, books, and conferences. He was an Associate Editor of the *IEEE TRANSACTIONS ON PATTERN ANALYSIS AND MACHINE INTELLIGENCE* and *Pattern Recognition* journals, and serves as an Associate Editor of the *Image and Vision Computing* journal. He was the President of the Pattern Recognition Society of Finland from 1989 to 1992. From 1989 to 2007, he served as a member of the Governing Board of the International Association for Pattern Recognition (IAPR), and became one of the founding fellows of IAPR in 1994.